Spin-Polarized Electronic Energy-Band Structure in EuS†

S. J. Cho*
Quantum Theory Project, University of Florida, Gainesville, Florida
(Received 10 November 1966)

The spin-polarized electronic energy bands for $Eu^{++}S^{--}$ have been calculated by using the augmented-plane-wave (APW) method. The results show that this material is a ferromagnetic as well as a semiconducting material. The muffin-tin crystal potential energy for the ionic form of $Eu^{++}S^{--}$, used to calculate the energy bands, is about 0.25 Ry higher than that for the case of neutral EuS. This influences the energy bands. The f bands for up spin are well localized with width 0.002 Ry, and are located 0.515 Ry below the top of the valence band Γ_{15}. On the other hand, the f bands for the down spin are conduction bands and are also localized, with a width of 0.031 Ry. These bands are located 0.115 Ry above the top of the valence band Γ_{15}. This quantity is also the direct band gap. At the zone center, the energy difference between these two f bands is 0.630 Ry. The bottom of the conduction band is located at the zone edge X, and the indirect transition occurs from the valence p band Γ_{15} to the conduction d band X_3 for up-spin electrons. The indirect energy gap obtained in this calculation is 0.111 Ry or 1.51 eV, compared with the experimental value 1.645 eV. This transition corresponds to the transition from the ground $3p$ shell in the S^{--} ion to the excited $5d$ shell in the Eu^{++} ion. The charge densities inside of the APW spheres have been analyzed, and are consistent with the energy-band picture. The constant-energy contours near the top of the valence band and near the bottom of the conduction band are shown.

INTRODUCTION

THE energy bands in europium sulfide have been studied by means of the augmented-plane-wave (APW) method.[1] The results show that EuS is a ferromagnetic as well as a semiconducting material, with no resemblance to the free-electron model. This is the first energy-band calculation for such a ferromagnetic and semiconducting material. Freeman *et al.*[2,3] investigated the electronic energy bands for the rare-earth metals, and found that the f bands are localized (energy width $=0.05$ eV for Gd). They also found that these f bands are located 0.8 Ry below the bottom of the $5d$-$6s$ bands, and that there is no resemblance to the free-electron model. However, there is rather strong resemblance to the transition metals due to the magnetic effect from the d conduction band. Since EuO was found to be ferromagnetic by Matthias, Borzorth, and Van Vleck,[4] a number of authors[5–7] have indicated that EuS and EuSe are also ferromagnetic, with transition temperatures of 16.5 and 7°K, respectively. On the other hand, EuTe is antiferromagnetic[7] at low temperature, and its paramagnetic susceptibility is practically constant between 1.6 and 4.2°K.[6] These europium compounds have the NaCl structure. They are of considerable interest from the theoretical and experimental viewpoints because of this simple structure and their ferromagnetic nature. Also, they are ideal materials to use in studying the magnetic properties of a half-filled Eu $4f$ shell. The magnetic moment for EuS is 6.87 μ_B at 0°K, and 6.67 μ_B at 4.2°K.[6] The spin-wave theory[8] and crystal-field theory[9,10] indicate that the first-order and second-order nearest exchange energies are given by $J_1/k=0.20$°K and $J_2/k=-0.08$°K, where k is the Boltzmann constant. The transition temperature and paramagnetic Curie points are determined by magnetic measurement and specific-heat anomaly. They are given in Table I. The Curie temperatures of Eu compounds decrease with increasing lattice constant.[6,10] EuS, EuO, and EuSe[11] are semiconductors at room temperature and below their Curie temperatures, and have a resistivity of the order of $10^7\ \Omega$ cm. In the paramagnetic temperature region, the absorption edge shifts towards

TABLE I. Experimental data for the NaCl-type series EuO, EuS, EuSe, and EuTe.

	EuO	EuS	EuSe	EuTe
Magnetic order	ferro.	ferro.	ferro-antiferro.	anti-ferro.
Lattice constant Å	5.144[a]	5.956[b]	6.173[b]	6.572[b]
Curie-Weiss temp. (°K)	76[a]	19[a]	9[a]	−6[a]
Molar Curie const.	7.60[a]	7.80[a]	7.33[a]	7.04[a]
μ_{eff}	7.81[c]	7.93[c]	7.70[c]	7.54[c]
Bohr magneton/Eu. at 0°K	6.80[a]	6.87[a]	6.70[a]	
Opt. band gap (eV) at RT	1.115[d]	1.645[d]	1.780[d]	1.050[d]
Critical temp. (°K)	69[a]	16.5[a]	7[a]	7.8[a]

[a] Taken from T. R. McGuire *et al.*, Ref. 6.
[b] Taken from W. B. Pearson, Ref. 24.
[c] Taken from S. Methfessel, Ref. 10.
[d] Taken from G. Busch *et al.*, Ref. 11.

† Supported by the National Science Foundation.
* Now at the National Research Council, Ottawa, Canada.
[1] J. C. Slater, Phys. Rev. **51**, 846 (1937).
[2] J. O. Dimmock and A. J. Freeman, Phys. Rev. Letters **13**, 750 (1964).
[3] A. J. Freeman, J. O. Dimmock, and R. E. Watson, Phys. Rev. Letters **16**, 94 (1966).
[4] B. T. Matthias, R. M. Bozorth, and J. H. Van Vleck, Phys. Rev. Letters **7**, 160 (1961).
[5] G. Busch, P. Junod, B. E. Risi, and O. Vogt, in *Proceedings of the International Conference on Semiconductors, Exeter, 1962* (The Institute of Physics and The Physical Society, London, 1962), p. 727.
[6] T. R. McGuire, B. E. Argyle, M. W. Schafer, and J. S. Smart, J. Appl. Phys. Letters **1**, 17 (1962); J. Appl. Phys. **34**, 1345 (1963); T. R. McGuire and M. W. Schafer, *ibid.* **35**, 984 (1964).
[7] S. Van Houston, Phys. Letters **2**, 215 (1962).
[8] S. H. Charap and E. L. Boyd, Phys. Rev. **133**, A811 (1964).
[9] S. Von Molnar and A. W. Lawson, Phys. Rev. **139**, A1598 (1965).
[10] S. Methfessel, Z. Angew. Phys. **18**, 414 (1965).
[11] G. Busch, P. Junod, and P. Wachter, Phys. Letters **12**, 11 (1964).

higher energies with decreasing temperature, but in the ferromagnetic region the absorption edge shifts towards lower energies for decreasing temperatures (below 20°K for EuO).[6,11,12] In the case of EuS, with spontaneous magnetization, the temperature dependence of the energy gap is $d(\Delta E_g)/dT = 1.7\times10^{-4}$ eV/deg (above the Curie point),[11] where E_g is the energy gap between conduction band and valence band. The optical energy gap for EuS is 1.645 eV at room temperature.[11]

The principal peak of the absorption shifts towards the longer wavelengths and becomes broader going from EuSe to EuS and EuO because of the effect of crystal field on the lattice constant.[13] Freeman *et al.*[14] show that the $4f$ electrons are shielded from the external crystalline field by the $5s$ and $5p$ electrons and that there are nonlinear deviations of the ordering and relative spacing of the crystal levels from the conventional $4f$ crystal field.

In this work, the spin-polarized Hartree-Fock-Slater atomic wave functions for the Eu^{++} and negative ion S^{--} are obtained by using a modified Herman-Skillman program.[15] The muffin-tin crystal potential for the ionic spin-polarized effect is also discussed, and one finds that the ionic case is about 0.25 Ry higher than that for the neutral case. The results of the energy-band calculations are consistent with available experimental data and physical phenomena. The $4f$ bands for the up spin are well localized and are located 0.515 Ry below the top of the valence bands. On the other hand, the f bands for the down spin are conduction bands and are also localized. They are located 0.115 Ry above the top of the valence bands, giving an energy separation between these two f bands of 0.630 Ry. The indirect transition occurs from the valence p band at the zone center to the conduction d band at the zone edge X for the up-spin electrons. The indirect gap obtained in this calculation is 0.111 Ry or 1.51 eV, as compared with the experimental value 1.645 eV. This corresponds to the transition from the ground-state $3p$ shell in S^{--} to the excited state of the $5d$ shell in Eu^{++} for the up-spin electrons. The charge density inside of the APW spheres at the zone center has been analyzed. The constant-energy contours near the top of the valence bands and near the bottom of the conduction bands are discussed.

ATOMIC WAVE FUNCTIONS

The atomic wave functions for the rare-earth elements have been extensively studied by Freeman and Watson.[14,16–19] In the present calculation, the self-consistent Hartree-Fock-Slater atomic equation with the $\rho^{1/3}$ free-electron model of the exchange potential energy[20] has been solved numerically by using the Herman-Skillman method.[15] The configurations of $(4d^{10}\ 4f^7\ 5s^2\ 5p^6)$ for Eu^{++} and $(3s^2\ 3p^6)$ for S^{--} have been used in this calculation. The spin polarization effect in Eu^{++} is also included by using a method similar to that described by Wood and Pratt.[21] The magnetic moment of Eu^{++} used in this calculation is 6.87 μ_B (see Table I). The radial charge densities for $4f$, $5s$, and $5p$ orbitals in Eu^{++} for up-spin and down-spin cases are shown in Fig. 1. The f orbitals are located well inside the $5s$ and $5p$ orbitals and are very localized. The maxima of the radial charge densities (Fig. 1) for the down-spin case are lower than the ones for the respective up-spin case by 9.8% for the $4f$ orbital, 3.1% for the $5s$ orbital, and 6.2% for the $5p$ orbital. The total radial charge density difference $\rho\uparrow-\rho\downarrow$ is shown in Fig. 2. It is interesting to compare the results obtained here with previous results obtained by Watson and Freeman for Gd^{+3}.[18] The $4f$, $5s$, and $5p$ radial charge densities for Eu^{++} are, in general, the same shape and their maxima and minima are located at the same positions as previous results for Gd^{+3}. However, the maximum for the up-spin $4f$ orbital in Eu^{++} is lower than for Gd^{+3}, although the $5s$ and $5p$ orbitals have about the same maxima, and overlap each other almost as in previous results. The difference in the radial charge density for up- and down-spin electrons is considerably different from that obtained by Watson and Freeman. Its shape and magnitude are similar to $\rho\uparrow-\rho\downarrow$ for the unfilled $4f$ shell of Watson and Freeman if we take into account the different numbers of electrons

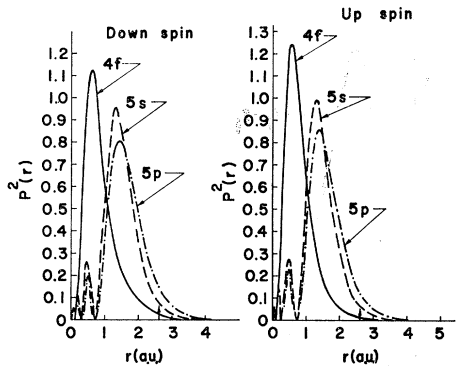

FIG. 1. Hartree-Fock-Slater radial charge densities for $4f$, $5s$, and $5p$ in the Eu^{++}.

[12] B. E. Argyle, J. C. Suits, and M. J. Freiser, Phys. Rev. Letters **15**, 822 (1965).
[13] J. C. Suits and B. E. Argyle, J. Appl. Phys. **36**, 1251 (1965).
[14] A. J. Freeman and R. E. Watson, Phys. Rev. **139**, A1606 (1965).
[15] F. Herman and S. Skillman, *Atomic Structure Calculations* (Prentice-Hall, Inc., Englewood Cliffs, New Jersey, 1963).
[16] R. E. Watson and A. J. Freeman, Phys. Rev. **133**, A1571 (1964).
[17] R. E. Watson and A. J. Freeman, Phys. Rev. Letters **6**, 277 (1961).
[18] A. J. Freeman and R. E. Watson, Phys. Rev. **127**, 2058 (1962).
[19] M. Blume, A. J. Freeman, and R. E. Watson, Phys. Rev. **134**, A320 (1964).
[20] J. C. Slater, Phys. Rev. **81**, 385 (1951).
[21] J. H. Wood and G. W. Pratt, Phys. Rev. **107**, 995 (1957).

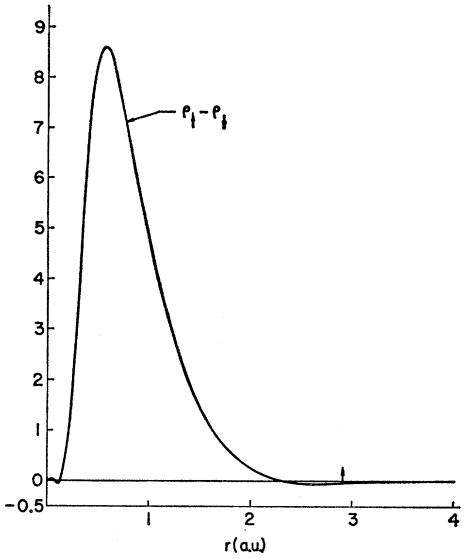

FIG. 2. Charge-density difference $\rho_\uparrow - \rho_\downarrow$ for the Eu^{++}.

in the f shell of Ge^{+3} and Eu^{++}, but its tail for Eu^{++} is considerably smaller than that for Gd^{+3}. The tail is negative, as is that of the Gd^{+3}, and the S^{--} ion sees a spin density opposite to the net spin of the Eu^{++}. There will be an exchange interaction between the up-spin electrons in S^{--} and the negative net spin of Eu^{++} due to the Pauli exclusion principle.

The self-consistent Hartree-Fock-Slater wave equation for S^{--} is also solved numerically by using an effective ionic radius of 1.84 Å,[22] as described by Watson,[23] and its results are shown in Fig. 3. The $3p$ wave function in S^{--} is quite broad as was expected, because of the capture of the loosely bound $6s$ electrons

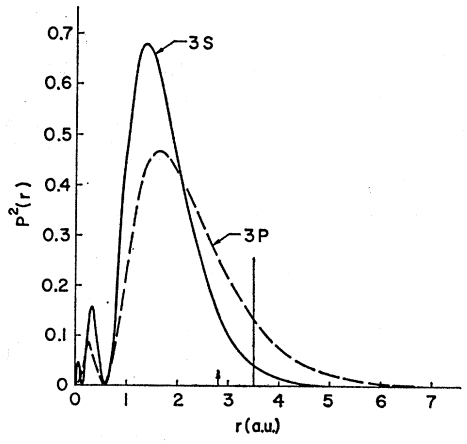

FIG. 3. Hartree-Fock-Slater radial charge densities for $3s$ and $3p$ in S^{--}.

[22] J. C. Slater, *Quantum Theory of Molecules and Solids* (McGraw-Hill Book Company, Inc., New York, 1965), Vol. 2, p. 99.

[23] R. E. Watson, Phys. Rev. **111**, 1108 (1958).

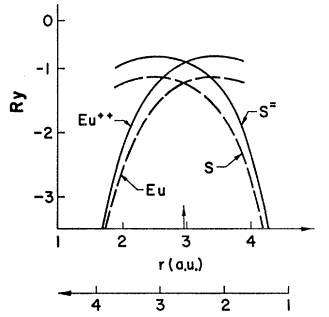

FIG. 4. Muffin-tin crystal potential energies for the ionic $Eu^{++}S^{--}$ and the neutral EuS, where ↑ denotes the crossing point. The upper abscissa is the distance measured from the Eu^{++} and the lower abscissa is the distance measured from the S^{--}.

from the Eu atom. The vertical line in Fig. 3 is the ionic radius for S^{--}. The arrows in Figs. 1–6 indicate the APW sphere radii. The $4f$ and $5s$ orbitals in Eu^{++} give a small contribution to the constant potential energy outside the APW sphere, as we see small tails in Fig. 1. The main contribution to the constant potential energy comes from the $5p$ orbital in Eu^{++} (see Fig. 1) and $3s$ and $3p$ orbitals in S^{--} (see Fig. 3). The atomic energy levels obtained by the Herman-Skillman method for S, S^{--}, Eu, Eu^{++}, $Eu^{++}(\uparrow)$, and $Eu^{++}(\downarrow)$ are tabulated in Table II.

CRYSTAL POTENTIAL ENERGY

The muffin-tin crystal potential energy for $Eu^{++}S^{--}$ is obtained by superimposing the free-ion charge densities described in the previous section for the spatial configuration of the NaCl structure. Referring to the Eu^{++} atom, there are six nearest neighbors of S^{--} ions at points $\pm\frac{1}{2}a(100)$, $\pm\frac{1}{2}(010)$, $\pm a(001)$; there are 12 next-nearest neighbors of Eu^{++} ions at $\pm\frac{1}{2}a(110)$, $\pm\frac{1}{2}a(1\bar{1}0)$, $\pm\frac{1}{2}a(011)$, $\pm\frac{1}{2}a(01\bar{1})$, $\pm\frac{1}{2}a(101)$, $\pm\frac{1}{2}a(10\bar{1})$, and so on, where a is the lattice constant, $a=5.957$ Å,[24]

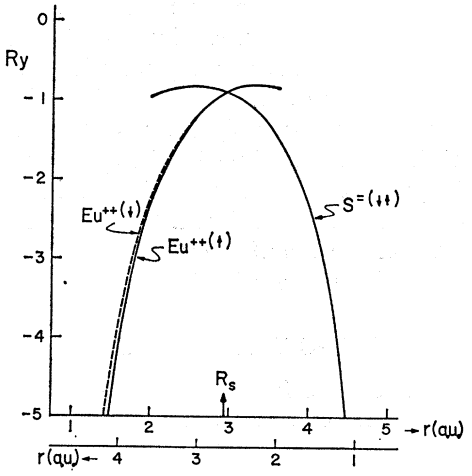

FIG. 5. Muffin-tin crystal potentiale nergies for up- and down-spin cases for $Eu^{++}S^{--}$. The upper abscissa is the distance measured from the Eu^{++} and lower abscissa is the distance measured from the S^{--}.

[24] W. B. Pearson, *A Handbook of Lattice Spacings and Structures of Metals and Alloys* (Pergamon Press, Inc., New York, 1958).

TABLE II. Atomic energy levels (in rydbergs) for S, S^{--}, Eu, Eu^{++}, $Eu^{++}(\uparrow)$, and $Eu^{++}(\downarrow)$.

	S	S^{--}		Eu	Eu^{++}	$Eu^{++}(\uparrow)$	$Eu^{++}(\downarrow)$
$2p$	−12.5470	−12.1507	$4d$	−10.8681	−11.8916	−12.145	−11.432
$3s$	−1.4756	−1.2207	$5s$	−3.2286	−4.2369	−4.368	−4.047
$3p$	−0.6956	−0.5139	$5p$	−2.0088	−3.0124	−3.117	−2.865
			$4f$	−1.0094	−2.0295	−2.267	−1.627
			$6s$	−0.3577			

for EuS. The first nine nearest-neighbor shells are included in this calculation. Because of the ionic nature of the crystal, we have to include the Madelung effect, $-4z\alpha/a$ ($\alpha=1.747558$ and z is the ionicity in units of electronic charges),[25] on the Coulomb potential. Let us consider an Eu^{++} ion located at the origin. The shell of ith-nearest neighbors (either Eu^{++} ions or S^{--} ions) contains N_i atoms at a radius R_i from the origin. Let z_i be the ionicity of this type of atoms. If we consider the crystal potential energy at an arbitrary point P which is located a distance r from the origin, the spherically averaged Coulomb potential energy $V_i(r)$ at P from an ion on this ith shell is obtained by using Löwdin's alpha-function expansion.[26]

$$\langle V_i(r)\rangle=\left\langle V_i(r)-\frac{z_i}{R_i}\right\rangle+\frac{z_i}{R_i}, \tag{1}$$

where $\langle f\rangle$ denotes the spherical average of $f(r)$. The total effective Coulomb potential energy at P from all ions except the one at the origin is expressed by

$$\tilde{V}(r)=\sum_{i=1}^{\infty}N_i\langle x_i(r)\rangle+\sum_{i=1}^{\infty}\frac{N_iz_i}{R_i}, \tag{2}$$

where $\langle x_i(r)\rangle=\langle V_i(r)-z_i/R_i\rangle$, and the second term is the Madelung correction, which can be replaced by $-4z\alpha/a$. The summation in the first term can be approximated by a finite number of shells. The final Coulomb potential energy at point P is then given by $V_c(r)=\tilde{V}(r)+V_0(r)$, where $V_0(r)$ is the Coulomb potential energy due to an ion at the origin. In this work the first nine shells have been included for this summation. Extra shells give negligible effect in the final results.

The APW sphere radius is determined by the crossing point of the Eu^{++} and S^{--} spherically averaged potential energies in the [100] direction. The sphere radii for Eu, S, Eu^{++}, and S^{--} are given in Table III. The crystal potential energies for EuS and $Eu^{++}S^{--}$ are shown in Fig. 4. As one can see from this figure, the ionic crystal potential energy for $Eu^{++}S^{--}$ is higher than the one for neutral EuS by about $\frac{1}{4}$ Ry over the whole unit cell. The up-spin and down-spin crystal potential energies for $Eu^{++}S^{--}$ are shown in Fig. 5. The maximum difference between up spin and down spin is 0.9 Ry and is shown in Fig. 6. This crystal potential energy difference is responsible for separating up-spin and down-spin f bands by 0.630 Ry as shown in Fig. 11. The exchange potential energy for the crystal potential is also approximated by $\rho^{1/3}$. The constant potentials outside the spheres for up-spin and down-spin electrons are obtained from average values of the crystal potentials in those regions, and are given in Table IV.

TABLE III. The APW sphere radii (in a.u.) for neutral EuS and for $Eu^{++}S^{--}$.

	EuS	$Eu^{++}S^{--}$
Eu	2.9519	2.9634
S	2.6767	2.6653

TABLE IV. Constant potential energies (in rybergs) between APW spheres for neutral EuS, and for $Eu^{++}S^{--}$ up- and down-spin cases.

EuS	$Eu^{++}S^{--}(\uparrow)$	$Eu^{++}S^{--}(\downarrow)$
−1.025	−0.6927	−0.6970

THE APW ENERGY-BAND CALCULATION

The APW method was first developed by Slater[1] and has been a leading method for determining the electronic energy bands in solids. It was first applied to copper by Chodorow[27] and later used by Wood[28] for iron, and by Burdick[29] for copper. Switendick[30] has extended

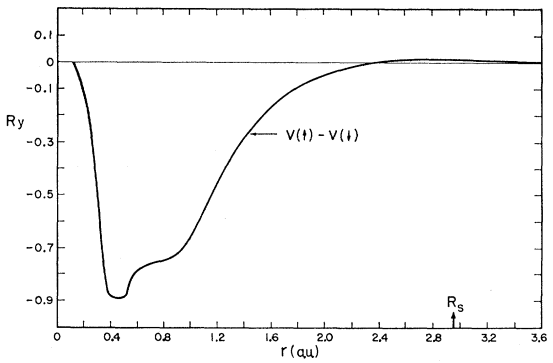

FIG. 6. Difference in the crystal potential energies for up spin and down spin in Eu^{++} in $Eu^{++}S^{--}$.

[25] C. Kittel, *Introduction to Solid State Physics* (John Wiley & Sons, Inc., New York, 1956), 2nd ed., p. 77.
[26] P.-O. Löwdin, Advan. Phys. **5**, 96 (1956).
[27] M. I. Chodorow, Ph.D. thesis, MIT, 1937 (unpublished).
[28] J. H. Wood, Phys. Rev. **117**, 714 (1960); **126**, 517 (1962).
[29] G. A. Burdick, Phys. Rev. **129**, 138 (1963).
[30] A. C. Switendick, Ph.D. thesis, Department of Physics, MIT, 1964 (unpublished).

this method to the problem of two atoms per unit cell in his energy-band calculation of NiO. De Cicco[31] used nonconstant potential energy outside of the APW spheres to study energy bands in KCl. Since then there have been a large number of applications to various crystals by many authors in the past few years. It is found that the APW method in most applications leads to good agreement with experimental evidence. The one-electron crystal potential energy associated with the APW method is generated in the muffin-tin form. That is, the potential is spherically averaged around each nucleus within a sphere of radius R_s and one chooses a constant potential energy between the spheres as described in the previous section. This potential energy, together with the periodic boundary contition, is used to solve the one-electron Schrödinger equation to give energy eigenvalues and APW functions. The computational procedure used in this calculation is similar to that described by Wood.[28] The radial wave functions $u_{l,p}(r,E)$ are determined by solving the radial Schrödinger equation for the potential energies in the different spheres for each up- and down-spin case, where index p refers to the pth sphere in the primitive cell.

The wave vectors $\mathbf{k}_i=\mathbf{k}+\mathbf{K}_i$ ($\mathbf{K}_i$ being the reciprocal lattice vectors) are those appropriate to each irreducible representation of the group of the reduced wave vector $\mathbf{k}$ in the first Brillouin zone. The matrix element ij corresponding to the wave vectors $\mathbf{k}_i$ and $\mathbf{k}_j$ of the secular determinant for a given energy and irreducible representation α is given[28] by

$$(H-E)_{ij}{}^{\alpha}=\sum_{R}\frac{G}{n_\alpha}\Gamma_\alpha{}^*(R)_{lm}\langle\psi_i|H-E|R\psi_j\rangle, \quad (3)$$

where G is the order of the group of the wave vector, $\{R\}$ is the set of operators of the group of the wave vector $\mathbf{k}$, n_α is the dimensionality of the irreducible representation α, $\Gamma_\alpha{}^*(R)_{lm}$ is the complex conjugate of the matrix element lm of the representation matrix corresponding to the group element R, and the matrix element $\langle\psi_i|H-E|R\psi_j\rangle$ for more than one atom per unit cell is given by Switendick.[30] (See Ref. 28 for other notations.)

RESULTS OF THE COMPUTATION

The energy-band calculation reported here is obtained using the potential energies shown in Fig. 5. No semiempirical adjustments of the constant potential outside the spheres have been made in this application. In this calculation one does not include the crystal-field effect and shielding effect, although they can affect the energy bands. The convergence tests of the secular equation indicate that the magnitude of the vector $\mathbf{k}$ in the range $80\leqslant|k|_{\max}{}^2\leqslant120$ produces energies accurate to within 0.001 Ry at the zone center. This corresponds

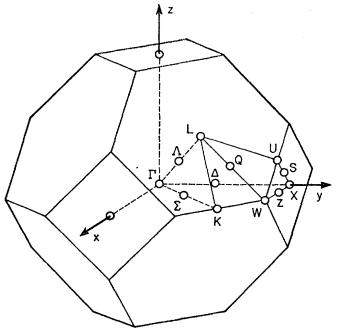

FIG. 7. Brillouin zone for fcc structure.

to 120 unsymmetrized plane waves. The expansion in spherical harmonics was taken up to $l=12$ (this test has been previously performed by Switendick[30]). The standard notation of Boukaert, Smoluchowski, and Wigner (BSW)[32] for various symmetry types has been used throughout this work, and the components of the wave vector $\mathbf{k}$ are given in units of π/a. It is necessary to compute the eigenvalues in one forty-eighth of the first Brillouin zone, the volume enclosed by surfaces ΓKWX, ΓLK, ΓXUL, $LKWU$, and WXU (see Fig. 7). The following points in this volume have been calculated: $\Gamma(0\,0\,0)$, $X(0\,2\,0)$, $\Delta(0\,\frac{1}{2}\,0)$, $\Delta(0\,1\,0)$, $\Delta(0\,\frac{3}{2}\,0)$, $\Lambda(\frac{1}{4}\,\frac{1}{4}\,\frac{1}{4})$, $\Lambda(\frac{1}{2}\,\frac{1}{2}\,\frac{1}{2})$, $\Lambda(\frac{3}{4}\,\frac{3}{4}\,\frac{3}{4})$, $L(1\,1\,1)$, $\Sigma(\frac{1}{4}\,\frac{1}{4}\,0)$, $\Sigma(\frac{1}{2}\,\frac{1}{2}\,0)$, $\Sigma(\frac{3}{4}\,\frac{3}{4}\,0)$, $\Sigma(1\,1\,0)$, $\Sigma(\frac{5}{4}\,\frac{5}{4}\,0)$, $K(\frac{3}{2}\,\frac{3}{2}\,0)$, $W(1\,2\,0)$, $Z(\frac{1}{2}\,2\,0)$. At $U(\frac{1}{2}\,2\,\frac{1}{2})$ the eigenvalues are identical to ones at $K(\frac{3}{2}\,\frac{3}{2}\,0)$.

Figure 8 shows the energy bands along the [100] direction for neutral and non-spin-polarized EuS. The

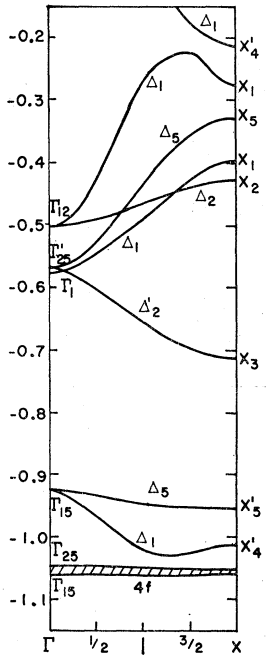

FIG. 8. Energy bands in the direction [100] for neutral EuS as a function of k.

[31] P. D. De Cicco, Ph.D. thesis, Department of Physics, MIT, 1965 (unpublished).

[32] L. P. Boukaert, R. Smoluchowski, and E. Wigner, Phys. Rev. **50**, 58 (1936).

f bands are highly localized as expected from the atomic charge densities shown in Fig. 1. Their bandwidth is 0.014 Ry, and they are located at 0.122 Ry below p band Γ_{15}. Figures 9 and 10 show the energy bands for up- and down-spin cases in $Eu^{++}S^{--}$ as a function of $\mathbf{k}$ along the paths Γ-K-W-X-Γ and Γ-L-U-X. It should be noted that the Γ_1 and Γ_{25}' conduction levels are in reverse order from the neutral case, and all the valence bands except the f bands are pushed up by about 0.4 Ry, which is about 1.6 times the difference in potential energy between the neutral and the spin-polarized case (see Fig. 4); on the other hand, all the conduction bands are pushed up about 0.25 Ry, which is about the same as the difference between the spin-polarized and neutral potential energies. The f bands (↑) are more localized than in the neutral case, with a width of 0.002 Ry. These f bands (↑) are located 0.515 Ry below the valence p band $\Gamma_{15}(\uparrow)$. This separation is 4.2 times that of the neutral case. The location of these f bands is almost the same as that of the neutral case. The indirect band gap $[\Gamma_{15}(\uparrow)-X_3(\uparrow)]$ for up-spin electrons is 0.111 Ry or 1.51 eV and the direct band gap $[X_5'(\uparrow)-X_3(\uparrow)]$ is 0.144 Ry or 1.96 eV. In the down-spin case, the f bands (↓) are conduction bands, as shown in Fig. 10, which we would expect because there are no down-spin electrons in the f orbital for the ground state in Eu^{++}. These conduction f bands (↓) are also well localized, although their width of 0.031 Ry at Γ is about 16 times larger than that for the up-spin case. The lowest of these bands, L_2', is located 0.134 Ry above the valence p band $\Gamma_{15}(\downarrow)$. This is also the direct band gap for the down-spin case.

Figure 11 shows the full energy bands for $Eu^{++}S^{--}$, both up- and down-spin cases. Individual f bands for up- and down-spin are not shown. They are Γ_2', Γ_{15}, Γ_{25}, Δ_1, Δ_2, Δ_2', $2\Delta_5$, X_2', X_3', X_4', $2X_5'$, L_1', $2L_2'$, L_3, $2L_3'$, $2\Lambda_1$, Λ_2, $2\Lambda_3$, $2K_1$, K_2, $2K_3$, $2K_4$, $2\Sigma_1$, Σ_2, $2\Sigma_3$, $2\Sigma_4$, W_1, W_2, W_2', $2W_3$, $2Z_1$, Z_2, $2Z_3$, $2Z_4$, where the numbers in front of the symbols are the number of times they appear in the f bands. As we see from this figure, the energy bands for down spin are, in general, higher than those for up spin. The band splittings due to the exchange polarization are tabulated in Table V. Negative signs in this table indicate energy bands for which the up-spin energy is higher than that for the down-spin electrons. The maximum and the minimum splitting between up-spin and down-spin f bands of the same symmetry occur at the zone center: $\Gamma_{15}(\uparrow)-\Gamma_{15}(\downarrow)=0.663$ Ry, and $\Gamma_2'(\uparrow)-\Gamma_2'(\downarrow)=0.630$ Ry. The other important band splittings are $L_2'(\uparrow)-L_2'(\downarrow)=0.019$ Ry for the valence s band, $X_4'(\uparrow)-X_4'(\downarrow)=0.021$ Ry for the valence p band, $X_5(\uparrow)-X_5(\downarrow)=0.113$ Ry for the conduction d band, $K_1(\uparrow)-K_1(\downarrow)=0.094$ Ry for the conduction s band, and $L_3(\uparrow)-L_3(\downarrow)=0.109$ Ry for the conduction d band. Band splittings due to the spin polarization decrease as one goes from Γ to W (see

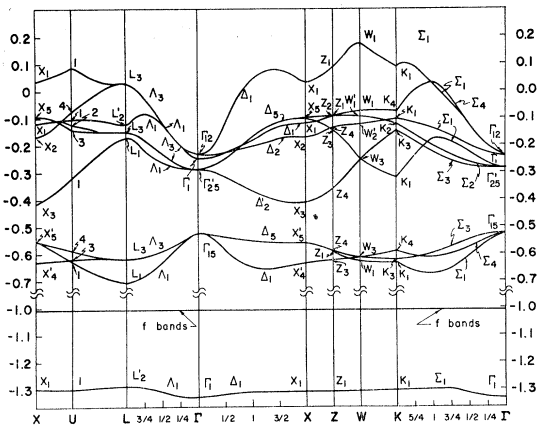

FIG. 9. Energy bands as a function of k for the up-spin case in $Eu^{++}S^{--}$.

TABLE V. Energy difference $\Delta E=E(\uparrow)-E(\downarrow)$ between up- and down-spin states due to the exchange polarization. The order is from lower to higher energies. Negative signs are for $E(\uparrow)>E(\downarrow)$. First column is the symmetry name, second column is the energy difference (in rydbergs), and third column designates major atomic states which contribute to the bands. Here we tabulate Γ, $\Delta(010)$, X, L, $\Lambda(\frac{111}{222})$, K, and $\Sigma(110)$ points.

	ΔE (Ry)			ΔE (Ry)			ΔE (Ry)			ΔE (Ry)	
Γ_1	0.004	s	X_2	0.091	d	Λ_1	0.632	f	K_4	0.637	f
	0.021	s	X_2'	0.638	f		0.644	f		0.644	f
Γ_2'	0.631	f	X_3	0.038	d		0.003	p		0.006	p
Γ_{15}	0.663	f	X_3'	0.635	f		0.055	d		0.069	d
	−0.019	p	X_4'	0.636	f		0.024	d	Σ_1	0.014	s
Γ_{25}	0.639	f		0.021	p	Λ_2	0.643	f		0.009	s
Γ_{12}	0.076	d	X_5	0.113	d	Λ_3	0.637	f		0.640	f
Γ_{25}'	0.060	d	X_5'	0.638	f		0.644	f		0.633	f
Δ_1	0.009	s		0.652	f		0.006	p		0.066	d
	0.639	f		−0.002	p		0.071	d		0.083	s
	0.009	p	L_1	0.012	p		0.081	d		−0.057	d
	0.047	s		0.064	d	K_1	0.007	s	Σ_2	0.635	f
Δ_2	0.637	f	L_1'	0.639	f		0.636	f		0.081	d
	0.083	d	L_2'	0.019	s		0.636	f	Σ_3	0.634	f
Δ_2'	0.634	f		0.632	f		0.010	p		0.641	f
	0.049	d		0.638	f		0.094	s		0.011	p
Δ_5	0.638	f		0.031	s		−0.039	d		0.050	d
	0.652	f	L_3	0.010	p	K_2	0.635	f	Σ_4	0.637	f
	−0.005	p		0.094	d		0.102	d		0.640	f
	0.082	d		−0.109	d	K_3	0.635	f		0.008	p
X_1	0.001	s	L_3'	0.634	f		0.638	f		−0.106	d
	0.084	d		0.642	f		0.019	p			
	−0.053	s	Λ_1	0.012	s		0.074	d			

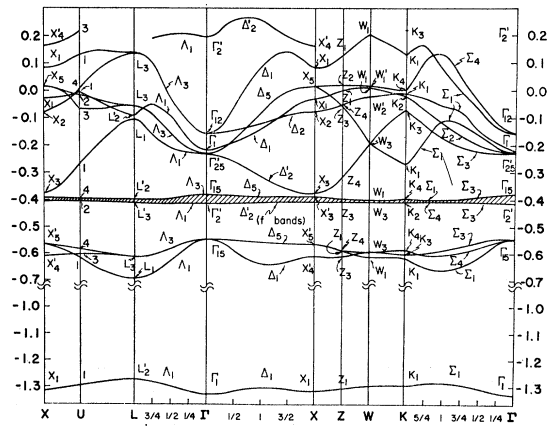

FIG. 10. Energy bands as a function of k for the down-spin case in $Eu^{++}S^{--}$.

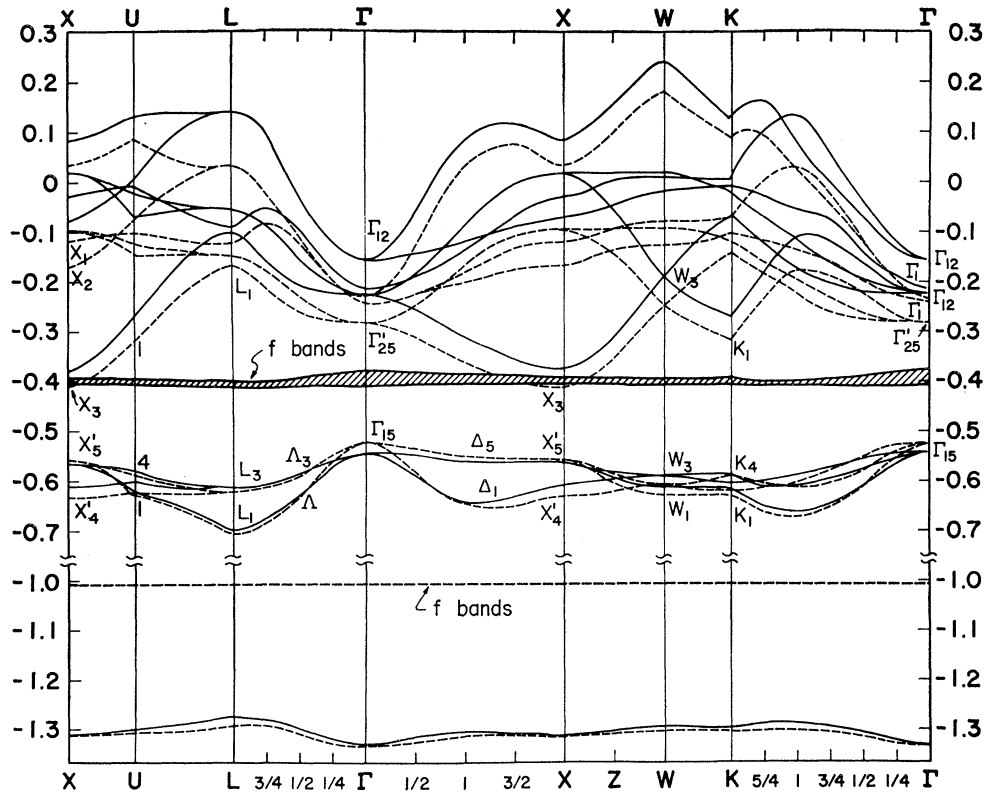

FIG. 11. Energy bands as a function of k for up- and down-spin cases in $Eu^{++}S^{--}$; dashed curve for up spin, and solid curve for down spin.

Table V for the complete listing). The top of the valence band occurs at the zone center for up spin. It is a $\Gamma_{15}(\uparrow)$ state, at -0.526 Ry. The bottom of the conduction band occurs at the zone edge X for up spin. It is an $X_3(\uparrow)$ state, at -0.415 Ry. The energy difference between these two bands is 0.111 Ry or 1.51 eV, which is the indirect band gap and compares to the experimental value of 1.645 eV.[11] This remarkable agreement is within the experimental error. From these energy bands we can say that the indirect transition occurs from valence band $\Gamma_{15}(\uparrow)$ to the conduction band $X_3(\uparrow)$. The energy difference for the direct transition between the $\Gamma_{15}(\uparrow)$ and the conduction f bands $(\downarrow)$ is 0.115 Ry or 1.56 eV, and it is 0.134 Ry or 1.82 eV between $\Gamma_{15}(\downarrow)$ and f bands $(\downarrow)$. These three types of the transitions are so close to each other that they may be difficult to distinguish in experiment. The f bands for down spin are not conduction bands in the usual sense, because this orbital in the Eu^{++} ion is well inside the $5s$ and $5p$ orbitals. However, these electrons have such high energies that they cannot stay in the f orbital and immediately transfer to the $5d$ orbital. The total energy bandwidths for the $3p$ band ($\Gamma_{15}-L_1=0.181$ Ry) and $5d$ band ($L_3-X_3=0.552$ Ry) are included in Table VI. It is interesting to compare the above $5d$ bandwidth with the $3d$ bandwidth in Fe (0.47 Ry)[28] and in Ni (0.360 Ry).[33] This comparison shows evidence of similarity between the $5d$ electrons in $Eu^{++}S^{--}$ and $3d$ electrons in Fe and Ni.

Ground states of the $Eu^{++}S^{--}$ have no conduction electrons. The conduction electrons arise from the thermal excitation of the electrons from the $3p$ shell in S^{--} to the $5d$ shell or $4f$ shell $(\downarrow)$ and are not from the f shell $(\uparrow)$ in Eu^{++} as mentioned by McClure,[34] based on the free-electron model. The following suggestions by McClure are not true: Conduction bands are not

TABLE VI. Energy bandwidth for p and d bands. The energy differences $\Gamma_{25}'-\Gamma_1$ and $\Gamma_1-\Gamma_{12}$ for the conduction bands are also given. First column for up spin, second column for down spin, and third column for maximum energy differences.

		$E(\uparrow)$(Ry)	$E(\downarrow)$(Ry)	E(Ry)
p	$\Gamma_{15}-L_1$	0.181	0.150	0.181
d	L_3-X_3	0.445	0.514	0.552
	$\Gamma_{25}'-\Gamma_1$	0.049	0.010	0.070
	$\Gamma_1-\Gamma_{12}$	0.018	0.063	0.084

TABLE VII. Comparison of calculated and experimental values for band gap (in eV).

Direct gap E_g (APW calculation)	Indirect gap E_{ig} (experimental)	Indirect gap E_{ig} (APW calculation)
1.56	1.645[a]	1.51

[a] Taken from G. Bush *et al.*, Ref. 11.

[33] S. Wakoh, J. Phys. Soc. Japan **20**, 1894 (1965).
[34] J. W. McClure, J. Phys. Chem. Solids **24**, 871 (1963).

TABLE VIII. Charge in the APW spheres for neutral EuS at the zone center (percent).

		In Eu sphere					In S sphere			
	Energy (Ry)	s	p	d	f	g	s	p	d	f
Γ_1	−0.578	19.6	···	···	···	0.47	16.2	···	···	···
Γ_2'	−1.051	···	···	···	99.6	···	···	···	···	0.02
Γ_{15}	−1.062	···	0.1	···	89.6	···	···	8.9	···	···
	−0.926	···	1.3	···	12.5	···	···	77.4	···	···
Γ_{25}	−1.047	···	···	···	99.8	···	···	···	···	···
Γ_{12}	−0.504	···	···	64.0	···	···	···	···	16.8	···
Γ_{25}'	−0.570	···	···	53.7	···	···	···	···	10.5	0.12

TABLE IX. Charge in the APW spheres for $Eu^{++}S^{--}$ (percent). These are for the up-spin case for Γ, L, and X.

		In Eu sphere					In S sphere			
	Energy (Ry)	s	p	d	f	g	s	p	d	f
Γ_1	−0.241	20.1	···	···	···	0.52	18.1	···	···	···
Γ_2'	−1.042	···	···	···	99.6	···	···	···	···	0.02
Γ_{15}	−1.043	···	···	···	99.3	···	···	0.4	···	···
	−0.526	···	1.4	···	2.7	···	···	84.3	···	···
Γ_{25}	−1.041	···	···	···	99.9	···	···	···	···	0.01
Γ_{12}	−0.233	···	···	70.4	···	···	···	···	16.8	···
Γ_{25}'	−0.290	···	···	61.0	···	···	···	···	10.5	0.12
L_1	−0.707	0.37	···	58.3	···	0.36	···	19.7	···	1.0
	−0.167	7.1	···	6.1	···	0.1	···	54.7	···	0.04
L_1'	−1.040	···	···	···	99.9	···	···	···	···	···
L_2'	−1.291	···	3.7	···	1.1	···	88.7	···	···	···
	−1.041	···	···	···	99.7	···	0.02	···	···	···
	−1.039	···	0.04	···	99.1	···	0.6	···	···	0.02
	−0.122	···	11.5	···	2.8	···	5.0	···	11.2	···
L_3	−0.623	···	···	16.3	···	0.2	···	67.0	···	0.1
	−0.149	···	···	78.4	···	0.1	···	3.1	···	1.3
	+0.029	···	···	73.1	···	0.2	···	20.6	···	1.3
L_3'	−1.041	···	···	···	99.7	···	···	···	···	0.04
	−1.040	···	···	···	99.8	···	···	···	···	0.04
X_1	−1.315	0.3	···	2.7	···	0.08	89.4	···	···	···
	−0.115	1.8	···	70.2	···	0.1	11.2	···	···	···
	+0.029	32.8	···	7.9	···	0.5	0.7	···	22.2	···
X_2	−0.168	···	···	77.4	···	0.05	···	···	11.9	···
X_2'	−1.041	···	···	···	99.8	···	···	···	···	···
X_3	−0.415	···	···	46.3	···	···	···	···	8.1	···
X_3'	−1.042	···	···	···	99.7	···	···	···	···	0.02
X_4'	−1.041	···	···	···	99.7	···	···	0.04	···	0.03
	−0.631	···	8.0	···	···	0.02	···	64.6	···	0.05
X_5	−0.095	···	···	87.2	···	···	···	···	0.1	0.5
X_5'	−1.042	···	0.01	···	99.5	···	···	0.3	···	···
	−1.041	···	···	···	99.8	···	···	···	···	0.02
	−0.559	···	4.0	···	1.6	···	···	78.3	···	0.03

TABLE X. Charge in the APW spheres for $Eu^{++}S^{--}$ (percent). These are for the down-spin case at the zone center.

		In Eu sphere					In S sphere			
	Energy (Ry)	s	p	d	f	g	s	p	d	f
Γ_1	−0.220	18.8	···	···	···	0.5	17.6	···	···	···
Γ_2'	−0.411	···	···	···	97.5	···	···	···	···	0.08
Γ_{15}	−0.545	···	1.3	···	14.4	···	···	73.3	···	···
	−0.380	···	0.25	···	87.2	···	···	11.6	···	0.07
Γ_{25}	−0.401	···	···	···	99.6	···	···	···	···	0.03
Γ_{12}	−0.157	···	···	64.1	···	···	···	···	16.0	···
Γ_{25}'	−0.230	···	···	53.5	···	···	···	···	9.8	···

mostly $6s$ orbitals on the rare-earth atom, but are due to $5d(\uparrow)$ and $f(\downarrow)$ orbitals. The bottom of the conduction band is not located at the zone center, but is located at the zone edge X. The energy gap is not from the $4f$ shell ($\uparrow$) to the bottom of the conduction band, but from the $3p$ shell ($\uparrow$) in S^{--} to the bottom of the conduction band.

The valence p band Δ_5 along the [100] direction is flat and higher than any other valence bands. This means all the direct and indirect transitions occur along this direction near the threshold energies. These transitions are from the valence p band (up spin or down spin) to the d band near the zone edge, or to down-spin f bands. The band gaps are tabulated in Table VII.

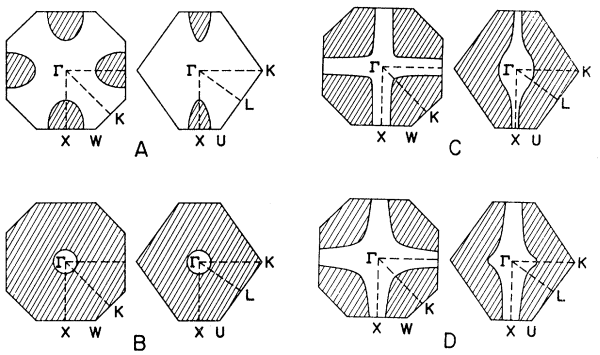

FIG. 12. Constant-energy contours for up-spin electrons in $Eu^{++}S^{--}$. (A) is for the conduction band at $E=-0.375$ Ry, and (B), (C), and (D) are for the valence bands at $E=-0.575$ Ry.

Other possible direct transitions at high symmetry points are $\Delta E(L_3(\downarrow)-f(\downarrow))=0.204$ Ry, $\Delta E(X_5'(\uparrow)-X_3(\uparrow))=0.144$ Ry, $\Delta E(W_3(\downarrow)-f(\downarrow))=0.191$ Ry, and $\Delta E(K_4(\downarrow)-f(\downarrow))=0.180$ Ry, where $f(\downarrow)$ indicates the f bands for down spin.

In general, there is more charge in the APW spheres for the up-spin case than the neutral case, although it reverses for the down-spin case. Tables VIII–X give the charge (in percent) inside the APW spheres for each band. The Γ_1 state in the conduction band for the up-spin case has only 38.2% of its charge inside of the APW spheres, and it is an admixture of the $6s$ orbital of Eu^{++} and the $4s$ orbital of S^{--}. The main parts of these s orbitals are well outside both Eu^{++} and S^{--} APW spheres. The valence p band Γ_{15} is mainly due to the $3p$ orbital in S^{--}, with a small admixture of the $5p$ and $4f$ orbitals of Eu^{++}. The up-spin f bands of Γ_2', Γ_{15}, and Γ_{25} have over 99% of their charge inside the APW spheres of Eu^{++} and are well localized, as we see in Fig. 11. However, the f band Γ_{15} for down spin has 12% less charge in the sphere than the up spin and is less localized. This causes the larger energy spread in the f bands for the down-spin case. The conduction bands

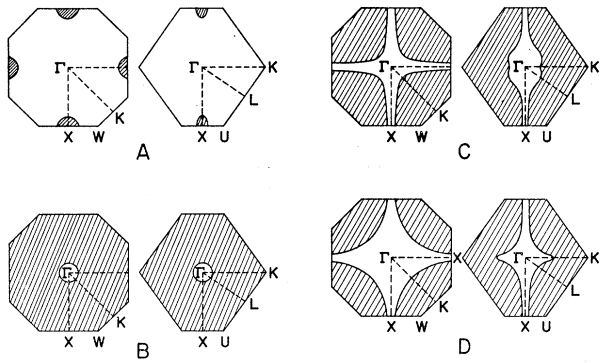

FIG. 13. Constant-energy contours for the down-spin electrons. (A) is for the conduction band at $E=-0.375$ Ry, and (B), (C), and (D) are for the valence bands for $E=-0.575$ Ry.

Γ_{12} and Γ_{25}' are mainly due to the excited $5d$ orbital in Eu^{++} with some admixture of the $3d$ orbital in S^{--}.

Figures 12 and 13 are the constant-energy contours due to the intersection between the constant-energy surfaces with the symmetry planes (100) and (110) through the point Γ. These are for the energy near the bottom of the conduction band, at $E=-0.375$ Ry, and near the maximum of the valence band, at $E=-0.575$ Ry. The shaded portions would be occupied by electrons having energies below those constant energies. The shape of the conduction band near the minimum is ellipsoidal as we see from Figs. 12(A) and 13(A). The lowest valence band has a nearly spherical surface at the zone center in the vicinity of its maximum [see Figs. 12(B) and 13(B)]. The other two upper valence bands have no intersection along the [100] directions, showing these bands to be flat along those directions.

DISCUSSION

The spin-polarized electronic energy-band calculation for the ferromagnetic $Eu^{++}S^{--}$ in terms of the APW method is consistent with available experimental results and physical phenomena. The muffin-tin crystal potential energy for ionic $Eu^{++}S^{--}$ is about 0.25 Ry higher than that for the neutral EuS. The indirect energy band gap obtained is 0.111 Ry or 1.51 eV compared to the experimental value 1.645 eV. The band gap for the direct transition is 0.115 Ry. The f bands for the up spin are valence bands, and are well localized at 0.515 Ry below the top valence p band Γ_{15}. On the other hand, the f bands for down-spin electrons are conduction bands and are also localized, at 0.115 Ry above the top of the valence band. The energy difference between those up and down f bands is 0.630 Ry, and the analysis of the charge inside of the APW spheres agrees well with localization of the f bands. The indirect transition is from the ground p shell in S^{--} to the excited d shell in the Eu^{++} ion, and the direct transition is from the ground p shell in S^{--} to f shell in Eu^{++}. These results are in contrast to those of McClure[34] based on the free-ion model, namely that the transition takes place from the f shell to the bottom of the conduction bands, and the conduction band mainly consists of the $6s$ orbitals in Eu^{++}. This energy-band calculation shows that $Eu^{++}S^{--}$ is a ferromagnetic and semiconducting material.

ACKNOWLEDGMENTS

The author wishes to thank Dr. James B. Conklin, Jr., for valuable discussions and careful reading of this paper. He also would like to thank Professor John C. Slater for his comments and continuous encouragement throughout this work. Finally, the author thanks John W. D. Connolly for his assistance. The use of the computing facilities of the University of Florida Computing Center is also acknowledged.